

# Probing spin textures in atomically thin CrSBr through tunneling magnetoresistance

Ziqi Liu<sup>1</sup>, Chengfeng Zhu<sup>1</sup>, Yuchen Gao<sup>1</sup>, Zuxin Chen<sup>2,\*</sup>, Pingfan Gu<sup>1,†</sup> and Yu Ye<sup>1,3,4‡</sup>

<sup>1</sup>*State Key Laboratory for Artificial Microstructure & Mesoscopic Physics and Frontiers Science Center for Nano-optoelectronics, School of Physics, Peking University, Beijing, 100871, China*

<sup>2</sup>*School of Semiconductor Science and Technology, South China Normal University, Foshan 528225, China*

<sup>3</sup>*Yangtze Delta Institute of Optoelectronics, Peking University, Nantong 226010 Jiangsu, China*

<sup>4</sup>*Liaoning Academy of Materials, Shenyang, 110167, China*

(Dated: July 19, 2024)

The exploration of spin configurations and magnetoresistance in van der Waals magnetic semiconductors, particularly in the realm of thin-layer structures, holds paramount significance for the development of two-dimensional spintronic nanodevices. In this Letter, we conducted comprehensive magnetotransport measurements on a few-layer CrSBr using a vertical tunneling device configuration. Notably, our investigation revealed that tunneling magnetoresistance possesses a distinctive capability to discern spin configurations that would otherwise remain indistinguishable through alternative techniques such as photoluminescence. We observed the existence of energy-degenerate states exhibiting identical net magnetization and comparable spin configurations, which could be differentiated based on their rectification properties, reminiscent of a diode-like behavior at positive and negative bias voltages. Specifically, in devices comprising 5-layer CrSBr, we observed an intriguing positive magnetoresistive state when subjected to an in-plane magnetic field along the  $b$ -axis. To gain a deeper understanding of the underlying mechanisms, we developed a one-dimensional linear chain model that successfully computed the magnetic state, thereby elucidating the underlying spin configurations responsible for the observed transport phenomena. These findings not only provide novel perspectives into the intricate spin textures of two-dimensional CrSBr but also underscore the sensitivity of tunneling as a probing technique for investigating the magnetic order in van der Waals materials.

## I. INTRODUCTION

Magnetic semiconductors play a crucial role in the field of condensed matter physics and materials science owing to their unique combination of semiconducting and magnetic properties [1–4]. This amalgamation presents promising opportunities for advances in spintronics, magnetic storage, and quantum computing [5–8]. The ability to manipulate both electrical current flow and magnetic moment orientation within a single material has great potential to improve the efficiency and versatility of electronic devices, with potential applications in energy-efficient electronics [9–12]. However, the controlled and stable realization of the desired combination of semiconducting and magnetic properties in materials remains a formidable challenge.

The recently discovered van der Waals (vdW) material CrSBr has garnered significant attention as a highly promising candidate due to its distinctive direct bandgap semiconductor characteristics and layered A-type antiferromagnetic (AFM) order [13]. Notably, CrSBr exhibits a pronounced spin-charge interaction, where its band

structure exhibits a strong dependence on its magnetic order through interlayer interactions [14]. Consequently, obtaining a comprehensive understanding of the evolution of spin textures in atomically thin CrSBr under external magnetic fields is of utmost importance for understanding the spin-charge interaction in a  $d$ -band hosting magnetic semiconductor, as well as for designing vdW AFM-based spintronic devices. Experimental investigations have demonstrated that below the Néel temperature of 132 K, CrSBr adopts an A-type AFM state [13]. Further studies have unveiled an intermediate ferromagnetic (iFM) state above the Néel temperature, characterized by intralayer ferromagnetic (FM) order and random interlayer magnetic order along the  $c$ -axis, with the critical temperature for intralayer magnetization ( $T_C^{\text{intra}}$ ) decreasing from  $\sim 160$  K in bulk to  $\sim 146$  K in monolayers [15, 16]. Moreover, zero-field muon spin rotation (ZF- $\mu$ SR) studies have indicated a deceleration of magnetic fluctuations below  $\sim 100$  K, with a spin freezing process occurring around 40 K [17]. Electrical transport and specific heat measurements have identified two additional magnetic phase transitions at higher temperatures (156 K and 185 K) [18], underscoring the intricate magnetic nature of CrSBr. Previous studies have reported layer-by-layer spin flips and overall spin-flop processes in few-layer CrSBr under an external magnetic field along the  $b$ -axis [14, 19]. However, the detailed mechanisms of each magnetic phase transition still remain unclear based

\* [chenzuxin@m.scnu.edu.cn](mailto:chenzuxin@m.scnu.edu.cn)

† [pingfangu@pku.edu.cn](mailto:pingfangu@pku.edu.cn)

‡ [ye\\_yu@pku.edu.cn](mailto:ye_yu@pku.edu.cn)

on the present experimental data.

Within the domain of vdW magnetic materials, particularly AFM semiconductors or insulators, the absence of a discernible magnetic moment necessitates the utilization of tunneling magnetoresistance as an effective and sensitive method for characterizing their magnetic properties [20, 21]. Variations in the band structure and material thickness resulting from magnetic phase transitions can influence the tunneling probability [2, 12, 19]. As tunneling probability is exponentially related to the barrier height and thickness of the material, slight changes can induce significant modifications in tunneling probability [22, 23]. Furthermore, the tunneling process has the ability to distinguish between degenerate magnetic states, since the tunneling barrier is influenced by both the bias voltage and the magnetic structure [24]. Given that the tunneling current is obtained by integrating the tunneling probability within the energy range that spans the Fermi levels of two metal contacts, thermal excitation has minimal impact on it [25].

This study delves into the investigation of spin configurations and magnetoresistance in few-layer CrSBr using vertical tunneling devices. When subject to an in-plane external magnetic field along the  $b$ -axis, CrSBr predominantly adopts colinear magnetic states, exhibiting a distinctive spin-flip evolution process during field sweeping. Notably, our measurements of tunneling magnetoresistance reveal spin configurations that are otherwise indistinguishable using alternative techniques. We also observe the presence of energy-degenerate states with identical magnetization but differing rectification behaviors under positive and negative biases. Surprisingly, in devices comprising 5-layer CrSBr, a positive magnetoresistive state appeared when an in-plane field was applied along the  $b$ -axis. To gain a deeper understanding of these phenomena, we develop a one-dimensional (1D) chain model that computes the magnetic states and elucidates the underlying spin textures that govern the transport properties. Overall, our findings provide novel insight into the intricate spin structure of CrSBr and underscore the sensitivity of tunneling as a probing technique for investigating magnetic order in van der Waals materials.

## II. RESULTS AND DISCUSSION

Single crystals of CrSBr are synthesized using the chemical vapor transport (CVT) technique and subsequently exfoliated into few-layer flakes using the conventional scotch tape method (see Methods). CrSBr possesses an orthorhombic lattice with cell dimensions of  $a=3.50$  Å,  $b=4.76$  Å, and  $c=7.96$  Å [16], where each CrSBr layer is stacked along the  $c$ -axis (Fig. 1a, b). Notably, CrSBr exhibits intralayer ferromagnetism along the  $b$ -axis, while interlayer A-type AFM coupling occurs along the  $c$ -axis (Fig. 1b). To investigate the magnetic transitions of CrSBr, we fabricated vertical tunneling devices based on few-layer CrSBr flakes (Fig. 1c). Cross-structured few-layer graphite stripes are employed to es-

tablish contact with the CrSBr tunneling layer, and the entire device is encapsulated by hexagonal boron nitride ( $h$ -BN, see Methods). The intentionally narrow width of the graphite layer aims to minimize the area of the tunneling junction, thereby reducing the impact of multi-domain effects in the junction area [19, 23]. The number of CrSBr layers is determined through atomic force microscope measurements (Supplementary Fig. S1).

Initially, the resistance of the devices was measured over a temperature range of 300 K to 2 K. Due to the semiconducting nature of CrSBr, the devices exhibited a resistance in the range of a few thousand ohms at room temperature (Fig. 1e). However, contrary to expectations based on typical semiconductor behavior, the device resistance did not show an exponential increase as the temperature decreased. Instead, a minor kink was observed at the Néel temperature ( $\sim 128$  K), indicating the emergence of AFM magnetic order [15, 16, 26]. Notably, the device resistance displayed a significant increase as the temperature decreased below 40 K, suggesting the dominance of the tunneling process (inset of Fig. 1e). This behavior may be associated with the spin-freezing process below 40 K [17]. Due to the strong in-plane anisotropy of CrSBr, the tunneling resistance exhibited precise  $180^\circ$  periodic symmetry when a small external magnetic field was applied and rotated in the  $ab$ -plane (Fig. 1f), providing a means to determine the orientation of the  $a$ - and  $b$ -axes (as confirmed by polarized Raman spectra in Supplementary Fig. S1d).

Following the determination of the  $a$ - and  $b$ -axes, the tunneling resistance was measured by sweeping a magnetic field along the  $a$ - or  $b$ -axis at a fixed bias voltage to investigate the magnetic behavior of the few-layer CrSBr. The magnetoresistance (MR) was calculated using the formula:

$$\text{MR} = \frac{R(B) - R(B=0)}{R(B=0)} \times 100\% \quad (1)$$

When a magnetic field was applied along the  $a$ -axis, the 4- and 5-layer CrSBr devices exhibited consistent behavior. Specifically, the tunneling resistance decreases with increasing magnetic field and eventually saturates, indicating a negative MR (Fig. 2a, c). This observation aligns with the magnetic ground state of CrSBr that magnetized along the  $b$ -axis, which features interlayer A-type antiferromagnetic. In the presence of an applied magnetic field, the magnetization of the layers gradually tilts towards the  $a$ -axis and eventually becomes fully magnetized along the  $a$ -axis [14]. In the FM state, the spin-up or spin-down electrons encounter lower tunneling barriers due to the uniform direction of magnetization in all CrSBr layers, resulting in significantly lower tunneling resistance than in the AFM state.

Nevertheless, when a magnetic field is applied along the  $b$ -axis, the 4- and 5-layer devices display distinct and unexpected transport properties, with each device undergoing a multistep spin-flip process. These transitions are accompanied by sharp changes in tunneling resistance

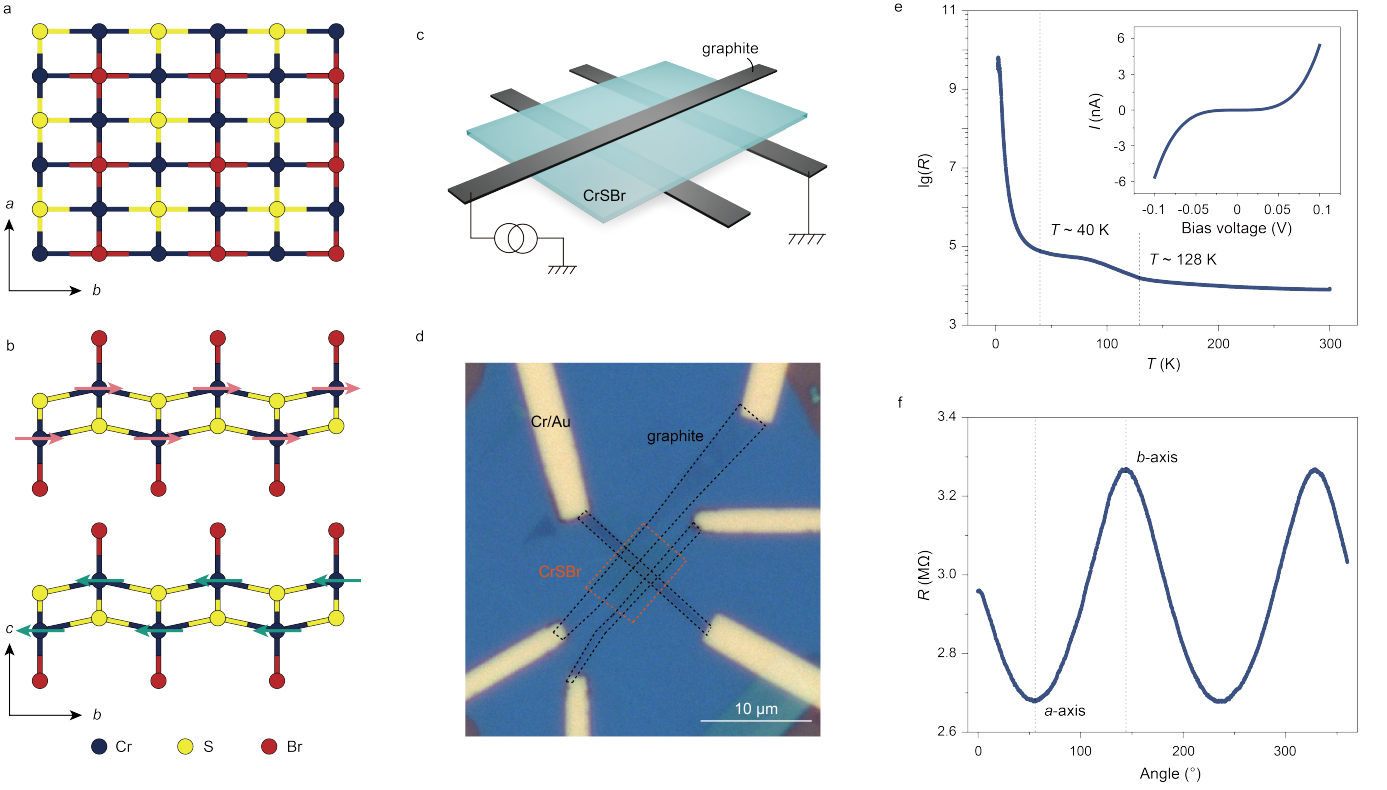


Figure 1. **Device structure and basic characterizations.** (a), Top view of the atomic structure of CrSBr. (b), Side view of the CrSBr atomic structure with arrows indicating the spin orientation of each Cr atom, revealing an A-type AFM ground state. (c, d), Schematic and optical image of the device. (e), Tunneling resistance of a 4-layer CrSBr device from 300 K to 2 K at a bias voltage of 10 mV. The dashed lines in the figure mark the two inflection points at 40 K and 128 K. The inset shows the  $I$ - $V$  curve of the device at 2 K. (f), Tunneling resistance of the device with an in-plane magnetic field. The angles of the magnetic field corresponding to the  $a$ - and  $b$ -axes are labeled in the figure. The bias voltage is 80 mV, and the magnitude of the magnetic field is 1 kG.

(Figs. 2b and d). In the case of the 4-layer CrSBr device, the material undergoes a transition from an A-type AFM state (high-resistance state) to an FM state (low-resistance state), resulting in a negative MR. Between the AFM and FM states, the tunneling resistance assumes an intermediate value, displaying significant hysteresis. Notably, at the same bias voltage and magnetic field, the tunneling resistance of the device exhibits two distinct resistance values during the ascending-field sweep and descending-field sweep, while the photoluminescence spectra display consistent exciton emission energy [14]. Similarly, in this intermediate state, the tunneling resistance displays two different values, low (high) and high (low), under negative and positive magnetic fields, respectively, during the ascending-field (descending-field) sweep (Fig. 2b).

In the case of the 5-layer device, a total of five distinct tunneling magnetoresistive states are observed during the evolution under a magnetic field along the  $b$ -axis. Taking the ascending-field sweep as an illustrative example, the device transitions from the low-resistance state of the FM phase (FM1) to a spin-flip intermediate resistive state (state1) and then to the high-resistance state of the AFM phase (AFM1) during the field's ascent. As

the positive magnetic field increases, the device enters another magnetic state (state 2) with even higher resistance than the AFM state, exhibiting a positive MR of up to 50%. Subsequently, it undergoes another spin-flip intermediate resistance state (state 3) to reach the FM low-resistance state (FM2) polarized along the positive magnetic field. It should be noted that the descending field process is a time-reversal process of the ascending field process (Fig. 2d).

To analyze the observed phenomena, a 1D linear chain model is employed to compute the magnetic state of CrSBr under an external magnetic field. The total energy of the CrSBr magnetic system is divided into three components: the AFM coupling between adjacent layers, the magnetic anisotropy energy, and the magnetization energy induced by the external field.

$$E = \sum_{i=1}^{n-1} J_{i,i+1} \cos(\varphi_{i+1} - \varphi_i) + \sum_{i=1}^n K_i \sin^2(\varphi_i) - \mu H \sum_{i=1}^n \cos(\varphi_i) \quad (2)$$

where  $\varphi_i$  represents the angle between the spin orientation of the  $i$ -th layer and the  $b$ -axis. We set  $J_{ij} = J = 1$ ,

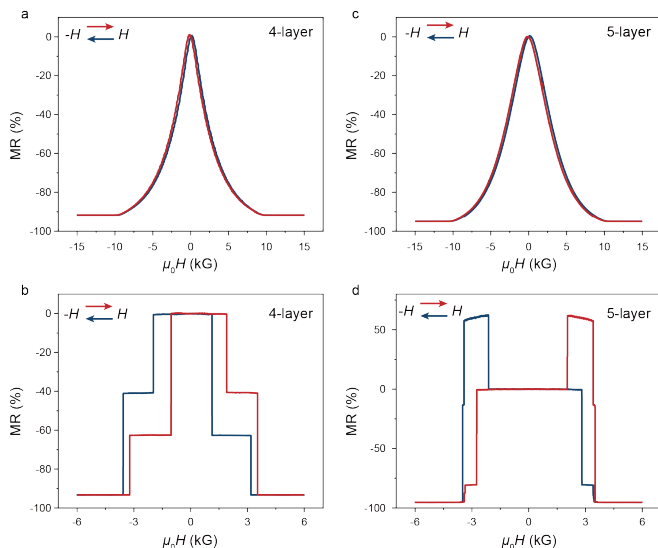


**Figure 2. Layer-dependent tunneling MR with magnetic field sweeping along the  $a$ - and  $b$ -axes.** (a), Tunneling resistance of a 4-layer CrSBr device with external magnetic field sweeping back and forth along the  $a$ -axis at 2 K and 70 mV bias voltage. (b), Tunneling resistance of the 4-layer CrSBr with the external magnetic field sweeping along the  $b$ -axis at 60 mV bias voltage. Two intermediate states with different resistance values are observed. (c), Tunneling resistance of a 5-layer CrSBr with the external magnetic field sweeping along the  $a$ -axis at 100 mV bias voltage. (d), Tunneling resistance of the 5-layer CrSBr with the external magnetic field sweeping along the  $b$ -axis at 100 mV bias voltage. A positive magnetoresistive state with an MR of 50% is observed.

$K_i = K = 1$  and  $\mu = 1$  in our model, consistent with previous studies [27]. Due to the significant magnetic anisotropy energy ( $K$ ) of CrSBr, the magnetic state evolution encounters formidable barriers. Recent studies have suggested that the evolution of the magnetic state in CrSBr may involve domain nucleation and the propagation of domain walls[28], enabling real systems to "leap" over these barriers. To address this, Monte Carlo and conjugate gradient descent methods are utilized to determine all stable magnetic states and compare their energies, thereby identifying the actual path of magnetic evolution. The actual evolutionary path involves a transition from a high-energy state to a low-energy state, with the Zeeman energy favoring the alignment of the magnetic moment parallel to the external magnetic field (Figs. 3a and b).

Here, we take the ascending-field sweep of the 4-layer CrSBr as an example (Figs. 3a and c), when subjected to a substantially large negative external magnetic field, the spin orientation of each layer aligns with the external field, exhibiting an FM (FM1,  $\downarrow\downarrow\downarrow\downarrow$ ) state along the  $b$ -axis. As the external field increases, one of the two middle layers undergoes a spin flip as an initial step to minimize the total energy by lowering the AFM coupling energy between the adjacent layers. Due to the device's asymmetric character, one of these two layers is

more likely to undergo the initial flip, reaching state 1 (e.g.,  $\downarrow\uparrow\downarrow\downarrow$ ). With a further increase of the external field, one surface layer also flips its spin orientation, causing CrSBr to reach the A-type AFM ground state (AFM1,  $\uparrow\uparrow\uparrow\downarrow$ ). As the magnetic field sweeps towards positive values, the surface spin-flip process flips the surface layer that is antiparallel to the magnetic field, transitioning CrSBr into state 2 ( $\uparrow\uparrow\downarrow\uparrow$ ). Subsequently, the spin orientation of the intermediate layer undergoes a flip, resulting in CrSBr transforming into an FM state aligned with the external field (FM2,  $\uparrow\uparrow\uparrow\uparrow$ ). The descending-field sweep represents a time-reversal operation of the ascending-field sweep, during which the 4-layer CrSBr goes through state 1' and state 2' (Fig. 3c).

It is worth emphasizing that state 1 and state 2 exhibit significantly different tunneling resistances, which cannot be distinguished by photoluminescence [14]. A toy model of the two-spin channel demonstrates that the tunneling barrier on each layer of CrSBr is modulated in the presence of a bias voltage (Supplementary Note S1), leading to a discrepancy in tunneling resistance between the two states (Fig. 3e). State 1' (state 2') represents the time-reversed counterpart of state 1 (state 2), and according to the two-spin channel model, it is expected to have the same tunneling resistance as state 1 (state 2), which was also confirmed in the experimental measurements (Fig. 2b). Notably, state 1 (state 2) and state 2' (state 1') are energetically degenerate states with identical net magnetization and similar spin configurations, but they can be differentiated based on their tunneling resistance. Ideally, reversing the current direction in these states would result in a change in their tunneling resistance, leading to rectification of the  $I$ - $V$  curve.

Similarly, in the case of a 5-layer CrSBr device during an ascending-field sweep, the initial FM state transitions to the AFM ground state through two sequential spin-flip processes. For the odd-layer samples, the uncompensated layer's net magnetization in the AFM state breaks the energy degeneracy under a non-zero external magnetic field. As the positive external magnetic field increases, the spin orientations of both surface layers align in the opposite direction to the external field. With further increase of the magnetic field, the spins of the two surface layers flip one after the other, followed by the spin of the intermediate layer, leading to the sample transitioning into the FM state, magnetized according to the direction of the magnetic field. The descending-field sweep represents the time-reversal process of the ascending-field sweep (Fig. 3d). However, while the spin configurations during the field sweep have been determined, the underlying cause of positive MR in the  $\downarrow\downarrow\uparrow\downarrow\downarrow$  ( $\uparrow\uparrow\downarrow\uparrow\downarrow$ ) magnetic state remains unknown. The two-spin channel model provides unconventional insights, suggesting a more complex origin. First, there is a one-to-one correspondence between the spin configuration and the band structure in this material, with certain spin configurations potentially having larger energy band gaps, leading to increased tunneling barriers [29]. Secondly, the charge transfer resulting from the difference in work functions between CrSBr and

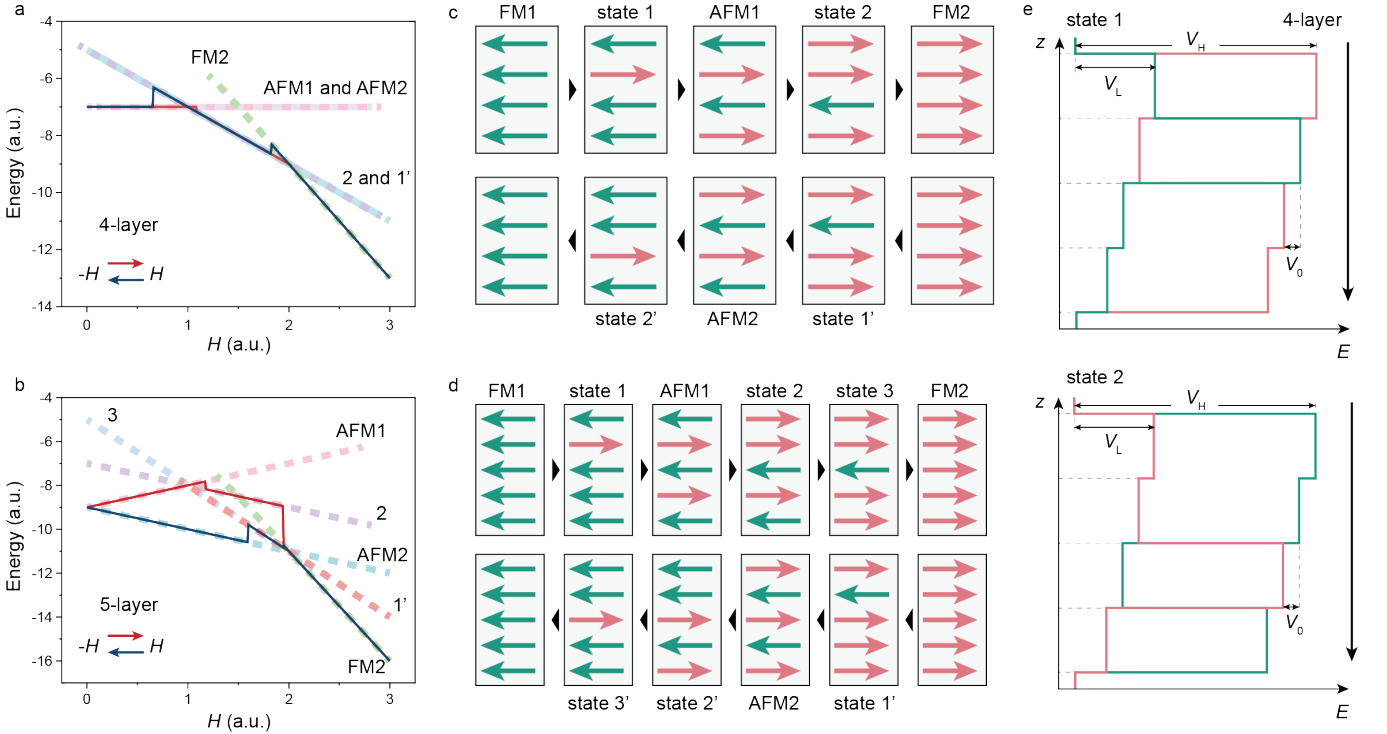


**Figure 3. 1D linear chain model and tunneling model.** (a), Calculated results of the 1D linear chain model for the 4-layer CrSBr. The red and blue lines represent the magnetic evolution process for ascending and descending field sweeps starting from the AFM state, respectively. The background dashed lines indicate the calculated energy variations of the steady states with the external magnetic field during the evolution process. (b), Calculated results of the 1D linear chain model for 5-layer CrSBr. All lines have the same meaning as in (a). (c), Schematic diagram illustrating the evolution of the spin configuration of the 4-layer CrSBr with the magnetic field. The green and orange arrows indicate the spin direction of each layer of CrSBr. The black triangles indicate the ascending and descending field processes. (d), Schematic diagram illustrating the evolution of the spin configuration of the 5-layer CrSBr with the magnetic field. (e), Schematic diagrams of the tunneling barriers for the spin-up (orange) and spin-down (green) electrons in the 4-layer CrSBr devices in state 1 and state 2. The directions of electron tunneling are indicated by the black arrows.

graphite may influence the spin-filtering effect of CrSBr in close proximity to the graphite layer, resulting in positive MR. Additionally, the proximity effect [30] caused by the strong spin-orbit coupling of CrSBr in graphite may also impact the MR of the tunneling junction. The specific reasons for this phenomenon require further investigation, and a more detailed discussion can be found in the Supplementary Note. S2. Due to the asymmetry of the spin configurations, reversing the current direction in the  $\downarrow\uparrow\downarrow\downarrow$  and  $\uparrow\uparrow\downarrow\downarrow$  states leads to two additional tunneling resistances (Supplementary Fig. S2).

To further confirm the evolution of the magnetic state, we performed measurements of the  $I$ - $V$  curves while sweeping the magnetic field (Figs. 4a and b). In both the 4-layer and 5-layer CrSBr devices, all asymmetric spin configurations exhibit a distinct diode-like rectification feature, indicating different tunneling resistances under positive and negative bias voltages. Importantly, this rectification behavior is determined by the spin configuration dictated by the magnetization history and is not influenced by the voltage sweeping history (Supplementary Fig. S3). The rectification ratio of the device depends on the specific magnetic configuration (Supple-

mentary Note 1); for instance, state 1 and state 2 in the 4-layer sample display opposing rectification ratios. Additionally, certain asymmetric resistances at positive and negative bias voltages observed in the 4- and 5-layer CrSBr devices, which remain constant irrespective of the magnetization history, may arise from device asymmetry or discrepancies between the two graphite electrodes.

To provide further information of the above-mentioned magnetic states, we conducted tunneling MR measurements on a 5-layer CrSBr device at different temperatures (Fig. 4c). As the temperature increases, a significant decrease in the tunneling resistance ratio between the AFM and FM states is observed. Simultaneously, the magnitude of the positive MR decreases and eventually disappears at  $\sim 10$  K, leaving only a minor negative MR component akin to the 4-layer CrSBr device. This result suggests that the plateaus of positive MR may be related to new emergent phases at low temperatures and susceptible to thermal fluctuations. Next, we investigated the MR behavior as a function of the in-plane magnetic field direction (Fig. 4d). Notably, the flip field of the magnetic state shows slight variation following the variable temperature measurements, which could be attributed to struc-

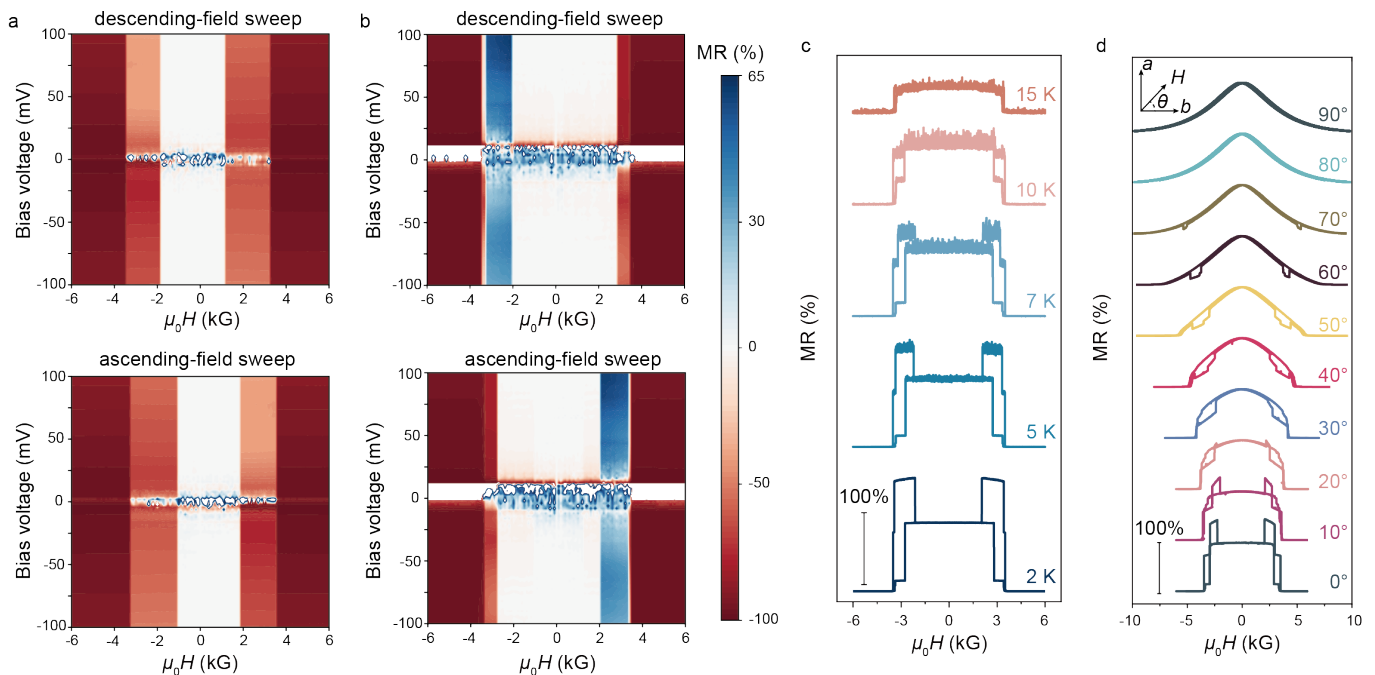


Figure 4. **Rectification properties of asymmetric spin configurations and evolution of magnetic states with temperature and magnetic field direction.** (a),  $I$ - $V$  curve mapping of a 4-layer CrSBr device under the external magnetic field along the  $b$ -axis descending-field (upper panel) and ascending-field (lower panel) sweeps. (b),  $I$ - $V$  curve mapping of a 5-layer CrSBr device under the external magnetic field along the  $b$ -axis descending-field (upper panel) and ascending-field (lower panel) sweeps. MR values near zero bias voltage are noisy due to the measurement resolution limit. (c), Temperature-dependent tunneling resistance of a 5-layer CrSBr device along the  $b$ -axis magnetic field. The bias voltages are 100 mV at 2 K, 5 K, and 7 K, 80 mV at 10 K, and 50 mV at 15 K. (d), Tunneling resistance of a 5-layer CrSBr device as a function of the magnetic field direction during rotation of the external magnetic field from the  $b$ -axis to the  $a$ -axis. The angle labeled in the figure represents the angle between the magnetic field direction and the CrSBr  $b$ -axis. The bias voltage is 100 mV.

tural changes in magnetic domains or defects. As the external magnetic field direction rotates from the  $b$ -axis to the  $a$ -axis, the spin orientation of CrSBr undergoes a tilting transition during the field sweep (Supplementary Fig. S4). Consequently, the magnitude of the positive MR diminishes as the external magnetic field deviates from the  $b$ -axis, while the spin tilt of the state becomes more pronounced. With further increase in the rotation angle, the positive MR state gradually transitions into a negative MR state and eventually disappears. Since this positive MR phenomenon has not been previously observed in reported CrSBr tunneling devices [2, 12, 21, 22, 24, 31], it signifies that the origin of positive MR is complex and requires further investigation.

In conclusion, our study investigated the magnetic properties and spin textures of few-layer CrSBr using tunneling magnetoresistance measurements. We identified distinct spin configurations that evolve with an in-plane magnetic field applied along different crystal axes. Notably, we observed energy-degenerate states that exhibited rectification behaviors under positive and negative biases. Intriguingly, a positive magnetoresistive state emerged in 5-layer CrSBr devices with a magnetic field along the  $b$ -axis. To gain insights into these phenomena, we developed a 1D chain model to compute the magnetic states, which helped to elucidate the underlying

spin textures responsible for the observed transport characteristics. Our findings provide novel insights into the complex spin structure of CrSBr, revealing subtle spin textures that are not easily discernible by other techniques. Furthermore, our work underscores the potential of tunneling magnetoresistance as a sensitive probe for investigating magnetic order in 2D materials. Further investigations focusing on spin dynamics and proximity effects in CrSBr heterostructures may unveil additional opportunities for spintronic applications.

### III. METHODS

**Crystal synthesis.** CrSBr single crystals were synthesized using the CVT method. Disulfur dibromide and chromium metal were mixed in a molar ratio of 7:13, and the mixture was sealed in a silica tube under vacuum conditions. Subsequently, the evacuated silica tube was inserted into a two-zone tubular furnace. The growth of CrSBr crystals took place over a period of 7 days, utilizing a temperature gradient ranging from 950 °C to 880 °C, with a controlled heating and cooling rate of 1 °C/min.

**Device fabrication.** Graphite,  $h$ -BN, and CrSBr flakes were exfoliated using the scotch tape method in ambient conditions and transferred onto a Si substrate covered with a 285

nm thick SiO<sub>2</sub> layer. The heterostructures were then stacked using a pick-up and release method based on a PPC/PDMS polymer stamp on a glass slide. Subsequently, the device underwent an acetone wash to remove PPC residual from the sample. A layer of poly methyl methacrylate (PMMA) was spin-coated and patterned using electron-beam lithography (EBL). The PMMA was developed using isopropyl alcohol, and the device was etched in a reaction-ion etching (RIE) system under O<sub>2</sub> and CHF<sub>3</sub> gas flow. Finally, Cr/Au electrodes, with a thickness of 5/35 nm were deposited on the device followed by a lift-off process to define metal contacts.

**Electrical measurements.** Transport measurements were

performed using a Heliox<sup>3</sup> He insert system equipped with a 14 T superconducting magnet, allowing temperature control down to 1.8 K. To analyze the *I-V* characteristics of the tunneling barrier and investigate the MR, a Keithley 2636B source meter was used to apply the bias voltage, while the tunneling current was measured using a standard two-probe module. To ensure the detection of intrinsic signals and minimize the impact of Joule heating, the tunneling current was limited to several hundreds of nA, resulting in a total power of several hundreds of nW in a junction with an approximate area of 1 μm<sup>2</sup>.

- 
- [1] T. Dietl, *Nature Materials* **9**, 965 (2010), ISSN 1476-4660, URL <https://doi.org/10.1038/nmat2898>.
- [2] Z. Wang, I. Gutiérrez-Lezama, N. Ubrig, M. Kroner, M. Gibertini, T. Taniguchi, K. Watanabe, A. Imamoglu, E. Giannini, and A. F. Morpurgo, *Nature Communications* **9**, 2516 (2018), ISSN 2041-1723, URL <https://doi.org/10.1038/s41467-018-04953-8>.
- [3] B. Huang, G. Clark, E. Navarro-Moratalla, D. R. Klein, R. Cheng, K. L. Seyler, D. Zhong, E. Schmidgall, M. A. McGuire, D. H. Cobden, et al., *Nature* **546**, 270 (2017), ISSN 1476-4687, URL <https://doi.org/10.1038/nature22391>.
- [4] C. Gong, L. Li, Z. Li, H. Ji, A. Stern, Y. Xia, T. Cao, W. Bao, C. Wang, Y. Wang, et al., *Nature* **546**, 265 (2017), ISSN 1476-4687, URL <https://doi.org/10.1038/nature22060>.
- [5] B. Huang, G. Clark, D. R. Klein, D. MacNeill, E. Navarro-Moratalla, K. L. Seyler, N. Wilson, M. A. McGuire, D. H. Cobden, D. Xiao, et al., *Nature Nanotechnology* **13**, 544 (2018), ISSN 1748-3387, 1748-3395, URL <https://www.nature.com/articles/s41565-018-0121-3>.
- [6] S. Jiang, L. Li, Z. Wang, K. F. Mak, and J. Shan, *Nature Nanotechnology* **13**, 549 (2018), ISSN 1748-3395, URL <https://doi.org/10.1038/s41565-018-0135-x>.
- [7] I. A. Verzhbitskiy, H. Kurebayashi, H. Cheng, J. Zhou, S. Khan, Y. P. Feng, and G. Eda, *Nature Electronics* **3**, 460 (2020), ISSN 2520-1131, URL <https://www.nature.com/articles/s41928-020-0427-7>.
- [8] Q. H. Wang, A. Bedoya-Pinto, M. Blei, A. H. Dismukes, A. Hamo, S. Jenkins, M. Koperski, Y. Liu, Q.-C. Sun, E. J. Telford, et al., *ACS Nano* p. acsnano.1c09150 (2022), ISSN 1936-0851, 1936-086X, URL <https://pubs.acs.org/doi/10.1021/acsnano.1c09150>.
- [9] J. Krempaský, G. Springholz, S. W. D'Souza, O. Caha, M. Gmitra, A. Ney, C. A. F. Vaz, C. Piamonteze, M. Fanciulli, D. Kriegner, et al., *Nature Communications* **14**, 6127 (2023), ISSN 2041-1723, URL <https://www.nature.com/articles/s41467-023-41718-4>.
- [10] K. Zhang, Y. Lee, M. J. Coak, J. Kim, S. Son, I. Hwang, D. Ko, Y. Oh, I. Jeon, D. Kim, et al., *Advanced Functional Materials* **31**, 2105992 (2021), ISSN 1616-301X, 1616-3028, URL <https://onlinelibrary.wiley.com/doi/10.1002/adfm.202105992>.
- [11] P. Gu, Y. Sun, C. Wang, Y. Peng, Y. Zhu, X. Cheng, K. Yuan, C. Lyu, X. Liu, Q. Tan, et al., *Nano Letters* **22**, 1233 (2022), ISSN 1530-6984, publisher: American Chemical Society, URL <https://doi.org/10.1021/acs.nanolett.1c04373>.
- [12] P. Gu, C. Wang, D. Su, Z. Dong, Q. Wang, Z. Han, K. Watanabe, T. Taniguchi, W. Ji, Y. Sun, et al., *Nature Communications* **14**, 3221 (2023), ISSN 2041-1723, URL <https://www.nature.com/articles/s41467-023-39004-4>.
- [13] O. Göser, W. Paul, and H. Kahle, *Journal of Magnetism and Magnetic Materials* **92**, 129 (1990), ISSN 03048853, URL <https://linkinghub.elsevier.com/retrieve/pii/030488539090689N>.
- [14] N. P. Wilson, K. Lee, J. Cenker, K. Xie, A. H. Dismukes, E. J. Telford, J. Fonseca, S. Sivakumar, C. Dean, T. Cao, et al., *Nature Materials* (2021), ISSN 1476-1122, 1476-4660, URL <http://www.nature.com/articles/s41563-021-01070-8>.
- [15] K. Lee, A. H. Dismukes, E. J. Telford, R. A. Wiscons, J. Wang, X. Xu, C. Nuckolls, C. R. Dean, X. Roy, and X. Zhu, *Nano Letters* **21**, 3511 (2021), ISSN 1530-6984, 1530-6992, URL <https://pubs.acs.org/doi/10.1021/acs.nanolett.1c00219>.
- [16] E. J. Telford, A. H. Dismukes, K. Lee, M. Cheng, A. Wieteska, A. K. Bartholomew, Y. Chen, X. Xu, A. N. Pasupathy, X. Zhu, et al., *Advanced Materials* **32**, 2003240 (2020), ISSN 0935-9648, 1521-4095, URL <https://onlinelibrary.wiley.com/doi/10.1002/adma.202003240>.
- [17] S. A. López-Paz, Z. Guguchia, V. Y. Pomjakushin, C. Witteveen, A. Cervellino, H. Luetkens, N. Casati, A. F. Morpurgo, and F. O. Von Rohr, *Nature Communications* **13**, 4745 (2022), ISSN 2041-1723, URL <https://www.nature.com/articles/s41467-022-32290-4>.
- [18] W. Liu, X. Guo, J. Schwartz, H. Xie, N. U. Dhale, S. H. Sung, A. L. N. Kondusamy, X. Wang, H. Zhao, D. Berman, et al., *ACS Nano* p. acsnano.2c02896 (2022), ISSN 1936-0851, 1936-086X, URL <https://pubs.acs.org/doi/10.1021/acsnano.2c02896>.
- [19] C. Ye, C. Wang, Q. Wu, S. Liu, J. Zhou, G. Wang, A. Söll, Z. Sofer, M. Yue, X. Liu, et al., *ACS Nano* **16**, 11876 (2022), ISSN 1936-0851, 1936-086X, URL <https://pubs.acs.org/doi/10.1021/acsnano.2c01151>.
- [20] J. Dong, X. Li, G. Gurung, M. Zhu, P. Zhang, F. Zheng, E. Y. Tsymbal, and J. Zhang, *Physical Review Letters* **128**, 197201 (2022), ISSN 0031-9007, 1079-7114, URL <https://link.aps.org/doi/10.1103/PhysRevLett.128.197201>.
- [21] D. R. Klein, D. MacNeill, J. L. Lado, D. Soriano, E. Navarro-Moratalla, K. Watanabe, T. Taniguchi, S. Manni, P. Canfield, J. Fernández-Rossier, et al.,

- Science **360**, 1218 (2018), ISSN 0036-8075, 1095-9203, URL <https://www.science.org/doi/10.1126/science.aar3617>.
- [22] B. Yang, T. Patel, M. Cheng, K. Pichugin, L. Tian, N. Sherlekar, S. Yan, Y. Fu, S. Tian, H. Lei, et al., Nature Communications **15**, 4982 (2024), ISSN 2041-1723, URL <https://www.nature.com/articles/s41467-024-49261-6>.
- [23] C. Boix-Constant, S. Jenkins, R. Rama-Eiroa, E. J. G. Santos, S. Mañas-Valero, and E. Coronado, Nature Materials (2023), ISSN 1476-1122, 1476-4660, URL <https://www.nature.com/articles/s41563-023-01735-6>.
- [24] Z. Fu, P. I. Samarawickrama, J. Ackerman, Y. Zhu, Z. Mao, K. Watanabe, T. Taniguchi, W. Wang, Y. Dahnovsky, M. Wu, et al., Nature Communications **15**, 3630 (2024), ISSN 2041-1723, URL <https://www.nature.com/articles/s41467-024-47820-5>.
- [25] J. J. Heath, M. Costa, M. Buongiorno-Nardelli, and M. A. Kuroda, Physical Review B **101**, 195439 (2020), ISSN 2469-9950, 2469-9969, URL <https://link.aps.org/doi/10.1103/PhysRevB.101.195439>.
- [26] E. J. Telford, A. H. Dismukes, R. L. Dudley, R. A. Wiscons, K. Lee, D. G. Chica, M. E. Ziebel, M.-G. Han, J. Yu, S. Shabani, et al., Nature Materials **21**, 754 (2022), ISSN 1476-1122, 1476-4660, URL <https://www.nature.com/articles/s41563-022-01245-x>.
- [27] K. Xie, X.-W. Zhang, D. Xiao, and T. Cao, ACS Nano **17**, 22684 (2023), ISSN 1936-0851, 1936-086X, URL <https://pubs.acs.org/doi/10.1021/acsnano.3c07125>.
- [28] J. Yu, D. Liu, Z. Ding, Y. Yuan, J. Zhou, F. Pei, H. Pan, T. Ma, F. Jin, L. Wang, et al., Advanced Functional Materials **34**, 2307259 (2024), ISSN 1616-301X, 1616-3028, URL <https://onlinelibrary.wiley.com/doi/10.1002/adfm.202307259>.
- [29] G. Long, H. Henck, M. Gibertini, D. Dumcenco, Z. Wang, T. Taniguchi, K. Watanabe, E. Giannini, and A. F. Morpurgo, Nano letters **20**, 2452 (2020).
- [30] T. S. Ghiasi, A. A. Kaverzin, A. H. Dismukes, D. K. de Wal, X. Roy, and B. J. van Wees, Nature Nanotechnology **16**, 788 (2021), ISSN 1748-3395, URL <https://www.nature.com/articles/s41565-021-00887-3>.
- [31] T. Song, X. Cai, M. W.-Y. Tu, X. Zhang, B. Huang, N. P. Wilson, K. L. Seyler, L. Zhu, T. Taniguchi, K. Watanabe, et al., Science **360**, 1214 (2018), ISSN 0036-8075, 1095-9203, URL <https://www.science.org/doi/10.1126/science.aar4851>.